PASSIVE INTELLIGENT SURFACE ASSISTED MIMO POWERED SUSTAINABLE IOT

Deepak Mishra

School of Electrical Engineering and Telecommunications
University of New South Wales (UNSW) Sydney
New South Wales (NSW) 2052, Australia

*Erik G. Larsson**

Department of Electrical Engineering
Linköping University
Linköping 581 83, Sweden

ABSTRACT

Lately, Passive Intelligent Surfaces (PIS) are being recognized to play an important role in meeting the timely demand of low-cost green sustainable Internet of Things (IoT). In this paper, we focus on maximizing the sum received power among the energy harvesting IoT users by jointly optimizing the active precoder for multi-antenna power beacon and the passive constant-envelope precoding based phase shifters (PS) design for PIS. Here, a multiuser channel estimation protocol is first introduced to obtain the least-squares estimators for the underlying effective cascaded channel links involved in the PIS assisted multi-antenna wireless power transfer as desired for the optimal precoder and PS designing. Thereafter, new semi-closed-form expressions for the proposed optimal active and passive beamforming design are derived so as to meet the low-complexity requirements of IoT communications. Finally, the numerical results are presented to validate the key nontrivial analytical claims and demonstrate the significant performance enhancement in terms of sum harvested energy among IoT users over conventional designs.

Index Terms— Wireless energy harvesting, passive beamforming, antenna array, channel estimation, least-squares, phase shifters.

1. INTRODUCTION

Passive intelligent surface (PIS) [1, 2], remotely programmed via a software controller, can alter the electromagnetic behavior of the wireless channel by appropriately reflecting a phase-shifted version of the incoming signal, without requiring any active radio resource for retransmission. However, the underlying major bottlenecks include unawareness about the ungoverned fading channel and ultra-low power computational capability. So, it is the need of the hour to investigate new constant-envelope constrained passive energy beamforming (EB) designs to gain smart system engineering perspectives.

1.1. State-of-the-Art

PIS is gaining significant research interest for supporting timely energy sustainability demands of wireless devices in Internet-of-things (IoT) [3–9]. Some of its implementation designs include lightweight elements attached to walls or ceilings [10], electronically-controlled resonant frequency based varactor diodes [11], and liquid crystal meta-surfaces fabricated via lithography or nanoprinting [5, 12].

Coming to more relevant works on passive EB designs for PIS, optimal transmit power allocation and phase shifters (PS) design was proposed in [9] for maximizing sum-rate. Considering energy harvesting (EH) users' individual signal-to-interference-plus-noise ratio (SINR) constraints during PIS-assisted multiple-input-single-output (MISO) energy transfer (PET), semidefinite relaxation (SDR) and alternating optimization techniques were used in [8] to obtain passive EB designs. Statistical channel state information (CSI) based study on the effect of PS design on the ergodic spectral efficiency was conducted in [13]. Investigating a PIS-assisted multiuser MISO system, two alternating optimization-based efficient energy efficiency maximization algorithms were proposed in [14]. In [15], the authors maximized the minimum SINR among mobile users via joint active and passive beamforming using random matrix theory tools. However, all these works either ignored low-complexity constraints of PIS or assumed perfect CSI availability. More recently, compressive sensing based channel construct approach to obtain the full CSI was presented in [16] and a least-squares (LS) based channel estimation (CE) protocol for single-user setting was developed in [17, 18]. But, *multiuser CE protocol involving low-complexity EB designs for maximizing sum power during PET* has not been investigated yet.

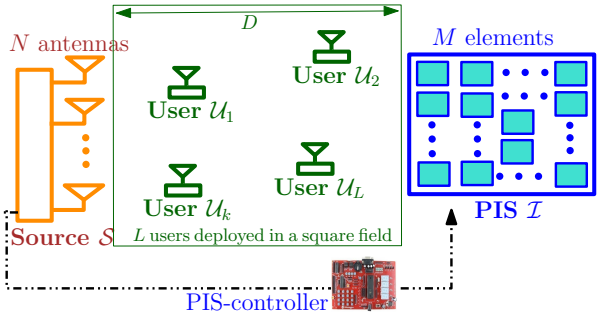

Fig. 1. Multiuser PET model with multiantenna energy source.

1.2. Motivation and Contributions

As the existing passive EB designs are based on computationally-inefficient numerical methods like SDR that do not provide any key system design insights, we aim to discourse *novel analytical expressions* for the jointly-optimal active and passive EB designs. We keep in mind the practical limitations like unavailability of strong prior for CE and overcoming PIS-bottlenecks by developing closed-form green PS designs to enable perpetual connectivity for sustainable IoT. The key contribution of this work is *three-fold*. (1) *Novel optimization framework and LS-based CE protocol* for the underlying effective cascaded channels are proposed to maximize the sum received power among multiple single-antenna IoT users during PET from a multiantenna power beacon (PB) (cf. Fig. 1). (2) *Nontrivial closed-form expressions* for the jointly-optimal active (transmit) precoder for PB and the passive (reflect) *constant-envelope precoding* based PS design for PIS to meet low-complexity requirements of IoT users. (3) A numerical investigation is carried out to *validate the key analytical claims and demonstrate the performance gains* over the benchmark. After outlining the system model in Section 2, these 3 contributions are respectively discoursed in Sections 3, 4, and 5.

*This work is supported by the Swedish Research Council and ELLIIT.

2. SYSTEM DESCRIPTION

2.1. Wireless Channel Model for Multiuser PET

We consider a multiuser MISO wireless system, where L single-antenna IoT users, $\mathcal{U} = \{\mathcal{U}_1, \mathcal{U}_2, \ldots, \mathcal{U}_L\}$, are randomly deployed inside a square-field of length D meters (m), with an N-antenna PB or energy source $\mathcal{S}$ [19], on one side of the field and an M-element PIS $\mathcal{I}$ installed on the opposite wall on the other side of the field, as shown in Fig. 1. With the flat quasi-static Rician block fading assumption, the channel impulse response for each link remains invariant during a coherence interval of τ seconds (s) and channels from PIS elements are assumed independent [2]. The baseband equivalent of fading coefficient for i-to-m link is represented by $\mathbf{H}_{im}$, $\forall i, m \in \{\mathcal{S}, \mathcal{U}, \mathcal{I}\}$, whose circularly symmetric complex Gaussian independent and identically distributed (i.i.d.) random entries have the same variance $\frac{\beta_{im}}{K_{im}+1}$ and different means as denoted by the matrix $\boldsymbol{\mu}_{im}$ modeling deterministic component [20] of i-to-m link, with its large-scale fading parameter as β_{im} and Rician factor as K_{im}.

2.2. Adopted PIS Design and Control

At PIS, its M passive elements [4, 9] function as M low-resolution PS which can be dynamically reconfigured via a PIS controller to control the scattering of the incident signals from $\mathcal{S}$ to the desired directions. The principal diagonal elements of diagonal PS matrix $\boldsymbol{\Theta} \in \mathbb{C}^{M\times M}$ as defined below represents the passive EB design and it includes $\alpha_i \in (0, 1)$ and $\theta_i \in (0, 2\pi)$ respectively denoting amplitude coefficient and PS value for each passive component i:

$$\boldsymbol{\Theta} \triangleq \operatorname{diag}\left\{\alpha_1 \mathrm{e}^{j\theta_1}\ \alpha_2 \mathrm{e}^{j\theta_2} \ldots \alpha_M \mathrm{e}^{j\theta_M}\right\}, \text{ with } j = \sqrt{-1}. \quad (1)$$

As shown in Fig. 1, PIS-controller adjusting αis and θis can be a micro-controller consuming ultra-low power, which is connected and programmed by $\mathcal{S}$ having all computational resources. Hence, the composite $\mathcal{S}$-to-$\mathcal{I}$-to-$\mathcal{U}$ channel involves the concatenation of $\mathcal{S}$-to-$\mathcal{I}$ channel $\mathbf{H}_{\mathcal{SI}}$, PS matrix $\boldsymbol{\Theta}$ at $\mathcal{I}$, and $\mathcal{I}$-to-$\mathcal{U}$ channel $\mathbf{H}_{\mathcal{IU}}$.

3. CHANNEL ESTIMATION FOR MULTIUSER PET

3.1. Channel-Reciprocity Based Downlink MISO PET

Since PIS is a passive reflecting unit, assuming channel-reciprocity and following the commonly investigated time-division duplex (TDD) communication mode in MISO systems [20, 21], the downlink (DL) channel coefficients for all links are obtained by estimating them from the uplink (UL) pilot transmission from the IoT users. We consider that each τs coherence interval is divided into two subphases, UL CE and DL PET. Therefore, with $\mathbf{f}_{\mathrm{A}} \in \mathbb{C}^{N\times 1}$ denoting the linear precoder or active EB vector at $\mathcal{S}$ and $x_e \in \mathbb{C}$ being its transmit energy signal having power $|x_e|^2 = p_e$, the combined signal $\mathbf{y}_{\mathcal{U}} \in \mathbb{C}^{L\times 1}$ received at IoT users during PET subphase is:

$$\mathbf{y}_{\mathcal{U}} = \left(\mathbf{H}_{\mathcal{SU}}^{\mathrm{T}} + \mathbf{H}_{\mathcal{IU}}^{\mathrm{T}}\, \boldsymbol{\Theta}\, \mathbf{H}_{\mathcal{SI}}^{\mathrm{T}}\right) \mathbf{f}_{\mathrm{A}}\, x_e + \mathbf{w}_{\mathcal{U}} = \Big(\mathbf{H}_{\mathcal{SU}}^{\mathrm{T}} + \mathbf{H}_{\mathcal{IU}}^{\mathrm{T}}\, \operatorname{diag}\{\mathbf{f}_{\mathrm{P}}\}\, \mathbf{H}_{\mathcal{SI}}^{\mathrm{T}}\Big) \mathbf{f}_{\mathrm{A}}\, x_e + \mathbf{w}_{\mathcal{U}} = \mathbf{G}\, \mathbf{f}_{\mathrm{A}}\, x_e + \mathbf{w}_{\mathcal{U}}, \quad (2)$$

where $\mathbf{G} \triangleq \mathbf{H}_{\mathcal{SU}}^{\mathrm{T}} + \mathbf{H}_{\mathcal{IU}}^{\mathrm{T}} \operatorname{diag}\{\mathbf{f}_{\mathrm{P}}\} \mathbf{H}_{\mathcal{SI}}^{\mathrm{T}} \in \mathbb{C}^{L\times N}$, M diagonal entries of $\boldsymbol{\Theta}$ in (1) form the passive EB or PS vector $\mathbf{f}_{\mathrm{P}} \in \mathbb{C}^{M\times 1}$ at $\mathcal{I}$, and $\mathbf{w}_{\mathcal{U}}$ is the received additive white Gaussian noise (AWGN) with zero-mean and variance $\sigma^2_{\mathrm{w}_{\mathcal{U}}}$. Next, ignoring the harvested energy from the noise power, the sum signal power as received among the L EH users can be approximated to $\mathcal{P}_{\mathcal{U}}$, as defined below:

$$\|\mathbf{y}_{\mathcal{U}}\|^2 \approx \mathcal{P}_{\mathcal{U}} \triangleq p_e \left\| \left(\mathbf{H}_{\mathcal{SU}}^{\mathrm{T}} + \mathbf{H}_{\mathcal{IU}}^{\mathrm{T}} \operatorname{diag}\{\mathbf{f}_{\mathrm{P}}\}\, \mathbf{H}_{\mathcal{SI}}^{\mathrm{T}}\right) \mathbf{f}_{\mathrm{A}} \right\|^2. \quad (3)$$

Since, the precoding vectors, $\mathbf{f}_{\mathrm{A}}$ and $\mathbf{f}_{\mathrm{P}}$ require the knowledge of CSI, next we outline LS method to obtain them via UL CE.

3.2. On-Off PIS Design Based Channel Estimation

Extending the CE protocol proposed for single-user settings in [17], we present a binary-reflection (*on* or *off*) based CE protocol for multiuser PET. Specifically, under this multiuser extension of the on-off model, PB estimates the CSI for all the links on an *element-by-element basis* at PIS over $M + 1$ subphases after obtaining the estimate for the direct $\mathcal{S}$-to-$\mathcal{U}$ channel matrix $\mathbf{H}_{\mathcal{SU}}$. In other words, only ith passive element of $\mathcal{I}$ is in *full-reflection or ON* mode with $\alpha_i = 1$ in $(i + 1)$st sub-phase, while all other elements, being in *no-reflection or OFF* mode, i.e., $\alpha_k = 0, \forall k \neq i$. Here, we use non-negative constants ϵ_1 and ϵ_0 respectively to model realistic implementation errors in *ON* and *OFF* modes. Therefore, the ith row and mth column entries of the combined PS matrix $\boldsymbol{\Phi} \in \mathbb{R}_{\geq 0}^{M\times(M+1)}$ during the CE phase are:

$$[\boldsymbol{\Phi}]_{i,m} \triangleq \begin{cases} 1 - \epsilon_1, & i = m + 1, \\ 0 + \epsilon_0, & \text{otherwise}, \end{cases} \quad \forall i \in \mathcal{M},\ m \in \mathcal{M}_+, \quad (4)$$

where $\mathcal{M} \triangleq \{1, 2, \ldots, M\}$ and $\mathcal{M}_+ \triangleq \mathcal{M} \cup \{M + 1\}$.

Next with p_c denoting the training average transmit power of each user $\mathcal{U}_i$ for each symbol period, the combined orthogonal pilot signal matrix can be represented by $\mathbf{X}_{\mathrm{p}} \in \mathbb{C}^{L\times L}$, which satisfies $\mathbf{X}_{\mathrm{p}} \mathbf{X}_{\mathrm{p}}^{\mathrm{H}} = p_c \tau_c\, \mathbf{I}_L$. Therefore, using (2), the combined received signal matrix $\mathbf{Y}_{\mathcal{S}} \in \mathbb{C}^{NL\times(M+1)}$ at $\mathcal{S}$ during CE can be written as:

$$\mathbf{Y}_{\mathcal{S}} = \Big(\left(\operatorname{vec}\{\mathbf{H}_{\mathcal{SU}}\, \mathbf{X}_p\} \otimes \mathbf{1}_{1\times(M+1)}\right) + \left((\mathbf{H}_{\mathcal{IU}}\, \mathbf{X}_p)^{\mathrm{T}} \otimes \mathbf{H}_{\mathcal{SI}}\right) \times \left[\operatorname{diag}\left\{\left[\boldsymbol{\Phi}^{\mathrm{T}}\right]_1\right\} \quad \boldsymbol{\mathcal{D}}_{\Phi}\right] \Big) + \mathbf{W}_{\mathcal{S}}, \quad (5)$$

where $[\mathbf{A}]_i$ is used to denote the ith row of matrix $\mathbf{A}$ and the operator $\otimes$ denotes the Kronecker product, $\mathbf{W}_{\mathcal{S}} \in \mathbb{C}^{NL\times(M+1)}$ is AWGN with variance $\sigma^2_{\mathrm{w}_{\mathcal{S}}}$ for all entries, and $\boldsymbol{\mathcal{D}}_{\boldsymbol{\Phi}} \in \mathbb{R}_{\geq 0}^{M^2\times M}$ is given by:

$$\boldsymbol{\mathcal{D}}_{\boldsymbol{\Phi}} \triangleq \left[\operatorname{diag}\left\{\left[\boldsymbol{\Phi}^{\mathrm{T}}\right]_2\right\} \operatorname{diag}\left\{\left[\boldsymbol{\Phi}^{\mathrm{T}}\right]_3\right\} \cdots \operatorname{diag}\left\{\left[\boldsymbol{\Phi}^{\mathrm{T}}\right]_{M+1}\right\}\right]^{\mathrm{T}}, \quad (6)$$

Here first and last M column vectors of $\mathbf{Y}_{\mathcal{S}}$ can be respectively separated as vector $\left[\mathbf{Y}_{\mathcal{S}}^{\mathrm{T}}\right]_1$ and matrix $\overline{\mathbf{Y}}_{\mathcal{S}} \in \mathbb{C}^{NL\times M}$ as defined below:

$$\left[\mathbf{Y}_{\mathcal{S}}^{\mathrm{T}}\right]_1 = \operatorname{vec}\left\{\left(\mathbf{H}_{\mathcal{SU}} + \epsilon_0\, \mathbf{H}_{\mathcal{SI}} \mathbf{1}_{M\times M} \mathbf{H}_{\mathcal{IU}}\right) \mathbf{X}_p\right\} + \mathbf{w}_1, \quad (7a)$$

$$\overline{\mathbf{Y}}_{\mathcal{S}} = \left(\operatorname{vec}\{\mathbf{H}_{\mathcal{SU}} \mathbf{X}_p\} \otimes \mathbf{1}_{1\times M}\right) + \left((\mathbf{H}_{\mathcal{IU}}\, \mathbf{X}_p)^{\mathrm{T}} \otimes \mathbf{H}_{\mathcal{SI}}\right) \boldsymbol{\mathcal{D}}_{\Phi} + \overline{\mathbf{W}}_{\mathcal{S}}, \quad (7b)$$

where with $\mathbf{w}_1 \triangleq \left[\mathbf{W}_{\mathcal{S}}^{\mathrm{T}}\right]_1 \in \mathbb{C}^{NL\times 1}$, $\mathbf{W}_{\mathcal{S}} = \left[\mathbf{w}_1 \ \ \overline{\mathbf{W}}_{\mathcal{S}}\right]$.

Therefore, the vectorized form $\operatorname{vec}\left\{\widehat{\mathbf{H}}_{\mathcal{SU}}\right\}$ of the LS estimate of $\mathcal{S}$-to-$\mathcal{U}$ channel matrix $\mathbf{H}_{\mathcal{SU}}$ as obtained using the pseudo-inverse $\mathbf{X}_{\mathrm{p}}^{\dagger} \triangleq \mathbf{X}_{\mathrm{p}}^{\mathrm{H}} \left(\mathbf{X}_{\mathrm{p}}\, \mathbf{X}_{\mathrm{p}}^{\mathrm{H}}\right)^{-1}$ of pilot signal $\mathbf{X}_{\mathrm{p}}$ is defined below [22]:

$$\operatorname{vec}\left\{\widehat{\mathbf{H}}_{\mathcal{SU}}\right\} = \left(\left(\mathbf{X}_{\mathrm{p}}^{\dagger}\right)^{\mathrm{T}} \otimes \mathbf{I}_N\right) \left[\mathbf{Y}_{\mathcal{S}}^{\mathrm{T}}\right]_1 = \operatorname{vec}\{\mathbf{H}_{\mathcal{SU}}\} + \operatorname{vec}\left\{\widetilde{\mathbf{H}}_{\mathcal{SU}}\right\}, \quad (8)$$

where the vectorized form of $\widetilde{\mathbf{H}}_{\mathcal{SU}}$ representing the CE error is:

$$\operatorname{vec}\left\{\widetilde{\mathbf{H}}_{\mathcal{SU}}\right\} = \epsilon_0 \operatorname{vec}\{\mathbf{H}_{\mathcal{SI}} \mathbf{1}_{M\times M} \mathbf{H}_{\mathcal{IU}}\} + \frac{\mathbf{X}_{\mathrm{p}}^{*} \otimes \mathbf{I}_N}{p_c \tau_c} \left[\mathbf{W}_{\mathcal{S}}^{\mathrm{T}}\right]_1. \quad (9)$$

Let us now define a matrix $\boldsymbol{\mathcal{G}} \triangleq \left(\mathbf{H}_{\mathcal{IU}}^{\mathrm{T}} \otimes \mathbf{H}_{\mathcal{SI}}\right) \boldsymbol{\mathcal{D}} \in \mathbb{C}^{NL \times M}$ and the underlying rectangular binary matrix $\boldsymbol{\mathcal{D}}$ is defined below:

$$\boldsymbol{\mathcal{D}} \triangleq [\mathbf{D}_1 \quad \mathbf{D}_2 \quad \mathbf{D}_3 \quad \cdots \quad \mathbf{D}_M]^{\mathrm{T}} \in \mathbb{B}^{M^2 \times M}. \tag{10}$$

Here $\mathbf{D}_i$ is a square-zero matrix with only it's ith principal diagonal element being 1, and $\mathbb{B} \triangleq \{0, 1\}$ is a set of binary numbers 0 and 1.

Next, using the LS estimate $\widetilde{\mathbf{H}}_{\mathcal{SU}}$ of $\mathbf{H}_{\mathcal{SU}}$ defined in (8), the LS estimate for the cascaded channel matrix $\boldsymbol{\mathcal{G}}$ is represented below:

$$\begin{aligned}\widehat{\boldsymbol{\mathcal{G}}} &= \left(\left(\mathbf{X}_{\mathrm{p}}^{\dagger}\right)^{\mathrm{T}} \otimes \mathbf{I}_N\right)\left(\overline{\mathbf{Y}}_{\mathcal{S}} - \left(\mathrm{vec}\left\{\widehat{\mathbf{H}}_{\mathcal{SU}}\mathbf{X}_p\right\} \otimes \mathbf{1}_{1\times M}\right)\right) \\ &= \left(\left(\mathbf{X}_{\mathrm{p}}^{\dagger}\right)^{\mathrm{T}} \otimes \mathbf{I}_N\right)\left(\left(\mathbf{H}_{\mathcal{IU}}\,\mathbf{X}_p\right)^{\mathrm{T}} \otimes \mathbf{H}_{\mathcal{SI}}\right)\boldsymbol{\mathcal{D}}_{\Phi} + \widetilde{\boldsymbol{\mathcal{G}}} \\ &= \left(\mathbf{H}_{\mathcal{IU}}^{\mathrm{T}} \otimes \mathbf{H}_{\mathcal{SI}}\right)\boldsymbol{\mathcal{D}}_{\Phi} + \widetilde{\boldsymbol{\mathcal{G}}}, \end{aligned} \tag{11}$$

where $\widetilde{\boldsymbol{\mathcal{G}}} \triangleq \left(\left(\mathbf{X}_{\mathrm{p}}^{\dagger}\right)^{\mathrm{T}} \otimes \mathbf{I}_N\right)\left(\overline{\mathbf{W}}_{\mathcal{S}} - \mathrm{vec}\left\{\widetilde{\mathbf{H}}_{\mathcal{SU}}\mathbf{X}_p\right\} \otimes \mathbf{1}_{1\times M}\right)$ representing error in estimating $\boldsymbol{\mathcal{G}}$ shows that CE in PET is more prone to errors than in conventional MISO communications without PIS. This critical aspect will be numerically verified in Section 5.2.

4. JOINTLY OPTIMAL ACTIVE AND PASSIVE EB DESIGN

Here first assuming perfect CSI availability at $\mathcal{S}$, we mathematically formulate the joint optimization problem $\mathcal{O}_{\mathrm{J}}$ of interest as below:

$$\begin{aligned}\mathcal{O}_{\mathrm{J}}: \max_{\mathbf{f}_{\mathrm{A}}, \mathbf{f}_{\mathrm{P}}} \quad & \mathcal{P}_{\mathcal{U}}, \qquad \text{subject to (s. t.) :} \\ & (\mathrm{C1}): \|\mathbf{f}_{\mathrm{A}}\|^2 \le 1, \qquad (\mathrm{C2}): \left|[\mathbf{f}_{\mathrm{P}}]_i\right| = 1, \forall i \in \mathcal{M}.\end{aligned}$$

Here note that, we set $\alpha_i = 1, \forall i \in \mathcal{M}$, to maximize the efficacy of PIS. Since $\mathcal{O}_{\mathrm{J}}$ is nonconvex, we next decouple it into two individual problems involving separate active and passive EB designing.

4.1. Optimal Active EB Design for a Given PIS Design

For a given PIS design $\mathbf{f}_{\mathrm{P}}$, active EB designing problem is given by:

$$\mathcal{O}_{\mathrm{A}}: \max_{\mathbf{f}_{\mathrm{A}}} \quad \|\mathbf{G}\,\mathbf{f}_{\mathrm{A}}\|^2 = \mathrm{Tr}\left\{\mathbf{G}\,\mathbf{f}_{\mathrm{A}}\,\mathbf{f}_{\mathrm{A}}^{\mathrm{H}}\,\mathbf{G}^{\mathrm{H}}\right\}, \quad \text{s. t. } (\mathrm{C1}).$$

Here it is not difficult to observe that the globally-optimal solution $\mathbf{f}_{\mathrm{A}}^{\mathrm{op}}$ of $\mathcal{O}_{\mathrm{A}}$ is characterized via the principal eigenvector $\mathrm{v}_{\max}\left\{\mathbf{G}^{\mathrm{H}}\,\mathbf{G}\right\}$ corresponding to the maximum eigenvalue $\lambda_{\max}\left\{\mathbf{G}^{\mathrm{H}}\,\mathbf{G}\right\}$ of matrix $\mathbf{G}^{\mathrm{H}}\,\mathbf{G}$. Therefore, $\mathbf{f}_{\mathrm{A}}^{\mathrm{op}} \triangleq \mathrm{v}_{\max}\left\{\mathbf{G}^{\mathrm{H}}\,\mathbf{G}\right\}$, and the maximum value of the objective of $\mathcal{O}_{\mathrm{A}}$ is bounded as:

$$\begin{aligned}\lambda_{\max}\left\{\mathbf{G}^{\mathrm{H}}\mathbf{G}\right\} \le \|\mathbf{G}\|^2 = \|\mathbf{H}_{\mathcal{SU}}\|^2 + \|\mathbf{H}_{\mathcal{SI}}\mathrm{diag}\left\{\mathbf{f}_{\mathrm{P}}\right\}\mathbf{H}_{\mathcal{IU}}\|^2 + \\ 2\,\mathrm{Re}\left\{\mathrm{Tr}\left\{\mathbf{H}_{\mathcal{SU}}^{\mathrm{H}}\mathbf{H}_{\mathcal{SI}}\mathrm{diag}\left\{\mathbf{f}_{\mathrm{P}}\right\}\mathbf{H}_{\mathcal{IU}}\right\}\right\}.\end{aligned} \tag{12}$$

Since $\mathbf{f}_{\mathrm{P}}$ is involved in the two terms $\|\mathbf{H}_{\mathcal{SI}}\,\mathrm{diag}\left\{\mathbf{f}_{\mathrm{P}}\right\}\,\mathbf{H}_{\mathcal{IU}}\|^2$ and $\mathrm{Tr}\left\{\mathbf{H}_{\mathcal{SU}}^{\mathrm{H}}\,\mathbf{H}_{\mathcal{SI}}\,\mathrm{diag}\left\{\mathbf{f}_{\mathrm{P}}\right\}\mathbf{H}_{\mathcal{IU}}\right\}$ of (12), next we propose two suboptimal designs based on individual optimization of each of them.

4.2. PS Design Maximizing Sum Received Power via PIS

This first PIS design is targeted to maximize the contribution of the second term in (12). Here, we first relax the nonconvex constant-envelope constraint (C2) to (C3) and the underlying PIS optimization problem reduces to:

$$\begin{aligned}\mathcal{O}_{\mathrm{P1}}: \max_{\mathbf{f}_{\mathrm{P}}} \quad & \|\mathbf{H}_{\mathcal{SI}}\,\mathrm{diag}\left\{\mathbf{f}_{\mathrm{P}}\right\}\mathbf{H}_{\mathcal{IU}}\|^2, \\ \text{s. t.} \quad & (\mathrm{C3}): \|\mathbf{f}_{\mathrm{P}}\|^2 \le M.\end{aligned}$$

Next, on associating the Lagrange multiplier $\nu_{\mathrm{P}_1} \ge 0$ with (C3), the Lagrangian function for $\mathcal{O}_{\mathrm{P1}}$ can be defined as:

$$\begin{aligned}\mathcal{L}_{\mathrm{P}_1} \triangleq \mathrm{Tr}\left\{\mathbf{H}_{\mathcal{SI}}\,\mathrm{diag}\left\{\mathbf{f}_{\mathrm{P}}\right\}\mathbf{H}_{\mathcal{IU}}\,\mathbf{H}_{\mathcal{IU}}^{\mathrm{H}}\,\mathrm{diag}\left\{\mathbf{f}_{\mathrm{P}}^{*}\right\}\mathbf{H}_{\mathcal{SI}}^{\mathrm{H}}\right\} \\ - \nu_{\mathrm{P}_1}\left(\|\mathbf{f}_{\mathrm{P}}\|^2 - M\right).\end{aligned} \tag{13}$$

and the underlying sub-gradient Karush-Kuhn-Tucker (KKT) condition [23], $\frac{\partial \mathcal{L}_{\mathrm{P1}}}{\partial \mathbf{f}_{\mathrm{P}}} = \mathbf{0}_{1\times M}$, is given by:

$$\mathbf{f}_{\mathrm{P}}^{\mathrm{H}}\boldsymbol{\mathcal{D}}^{\mathrm{T}}\left(\mathbf{H}_{\mathcal{IU}}^{*} \otimes \mathbf{H}_{\mathcal{SI}}^{\mathrm{H}}\right)\left(\mathbf{H}_{\mathcal{IU}}^{\mathrm{T}} \otimes \mathbf{H}_{\mathcal{SI}}\right)\boldsymbol{\mathcal{D}} - \nu_{\mathrm{P}_1}\mathbf{f}_{\mathrm{P}}^{\mathrm{H}} = \mathbf{0}_{1\times M} \tag{14}$$

which can be simplified to the eigenvalue problem form: $\boldsymbol{\mathcal{G}}\,\boldsymbol{\mathcal{G}}^{\mathrm{H}}\,\mathbf{f}_{\mathrm{P}} = \nu_{\mathrm{P}_1}\mathbf{f}_{\mathrm{P}}$. So, the globally-optimal solution of $\mathcal{O}_{\mathrm{P1}}$ can be characterized via the principal eigenvector corresponding to the maximum eigenvalue of matrix $\boldsymbol{\mathcal{G}}\,\boldsymbol{\mathcal{G}}^{\mathrm{H}}$. Thus, $\mathbf{f}_{\mathrm{P}}^{\mathrm{op1}} \triangleq \mathrm{v}_{\max}\left\{\boldsymbol{\mathcal{G}}\,\boldsymbol{\mathcal{G}}^{\mathrm{H}}\right\}$. However, as the optimal passive EB has to satisfy the practical PIS design constraint (C2), the first proposed low-complexity PIS design $\mathbf{f}_{\mathrm{P}}^{\mathrm{pr1}}$ can be obtained as the minimizer of the following optimization problem:

$$\mathcal{O}_{\mathrm{L}}: \min_{\mathbf{f}_{\mathrm{P}}} \quad \left\|\mathbf{f}_{\mathrm{P}} - \mathbf{f}_{\mathrm{P}}^{\mathrm{op1}}\right\|^2, \qquad \text{s. t.} \quad (\mathrm{C2}).$$

Therefore following [24, 25], the semi-closed-form expression $\mathbf{f}_{\mathrm{P}}^{\mathrm{pr1}}$ for the globally-optimal solution of $\mathcal{O}_{\mathrm{L}}$ in terms of $\mathbf{f}_{\mathrm{P}}^{\mathrm{op1}}$ that also satisfies the constant-envelope constraint (C2) on PIS design is:

$$\mathbf{f}_{\mathrm{P}}^{\mathrm{pr1}} \triangleq \exp\left\{j\,\angle\mathrm{v}_{\max}\left\{\boldsymbol{\mathcal{G}}\,\boldsymbol{\mathcal{G}}^{\mathrm{H}}\right\}\right\}, \tag{15}$$

where $\angle a = \tan^{-1}\left\{\frac{\mathrm{Im}\{a\}}{\mathrm{Re}\{a\}}\right\}$ denotes the phase angle operator.

4.3. Analytical PIS Design for Constructive Interference

The second low-complexity PIS design is aimed to ensure that the reflected signals from $\mathcal{I}$ get coherently added up at $\mathcal{U}$ with ones received directly from $\mathcal{S}$. This will result in the maximization of the third term in (12) and the underlying optimization problem is given by:

$$\mathcal{O}_{\mathrm{P2}}: \max_{\mathbf{f}_{\mathrm{P}}} \quad \mathrm{Tr}\left\{\mathbf{H}_{\mathcal{SU}}^{\mathrm{H}}\,\mathbf{H}_{\mathcal{SI}}\,\mathrm{diag}\left\{\mathbf{f}_{\mathrm{P}}\right\}\mathbf{H}_{\mathcal{IU}}\right\}, \qquad \text{s. t.} \quad (\mathrm{C3}).$$

Here also, on associating the Lagrange multiplier $\nu_{\mathrm{P}_2} \ge 0$ with (C3), the Lagrangian function for $\mathcal{O}_{\mathrm{P2}}$ can be revealed as:

$$\mathcal{L}_{\mathrm{P}_2} \triangleq \mathrm{Tr}\left\{\mathbf{H}_{\mathcal{SU}}^{\mathrm{H}}\mathbf{H}_{\mathcal{SI}}\,\mathrm{diag}\left\{\mathbf{f}_{\mathrm{P}}\right\}\mathbf{H}_{\mathcal{IU}}\right\} - \nu_{\mathrm{P}_2}\left(\|\mathbf{f}_{\mathrm{P}}\|^2 - M\right), \tag{16}$$

and the underlying subgradient KKT condition is given by:

$$\frac{\partial \mathcal{L}_{\mathrm{P}_2}}{\partial \mathbf{f}_{\mathrm{P}}} = \left(\mathrm{vec}\left\{\mathbf{H}_{\mathcal{SU}}\right\}\right)^{\mathrm{H}}\left(\mathbf{H}_{\mathcal{IU}}^{\mathrm{T}} \otimes \mathbf{H}_{\mathcal{SI}}\right)\boldsymbol{\mathcal{D}} - \nu_{\mathrm{P}_2}\mathbf{f}_{\mathrm{P}}^{\mathrm{H}} = \mathbf{0}_{1\times M}. \tag{17}$$

Solving above in $\mathbf{f}_{\mathrm{P}}$ leads to globally-optimal solution of $\mathcal{O}_{\mathrm{P2}}$ as:

$$\mathbf{f}_{\mathrm{P}}^{\mathrm{op2}} \triangleq \frac{1}{\nu_{\mathrm{P}_2}}\,\boldsymbol{\mathcal{G}}^{\mathrm{H}}\,\mathrm{vec}\left\{\mathbf{H}_{\mathcal{SU}}\right\}. \tag{18}$$

Now again here noting that scalar $\nu_{\mathrm{P}_2} \ge 0$, the closed-form expression for the optimal constant-envelope PIS design $\mathbf{f}_{\mathrm{P}}^{\mathrm{pr2}}$, satisfying (C2) as obtained by solving the underlying LS error $\left\|\mathbf{f}_{\mathrm{P}} - \mathbf{f}_{\mathrm{P}}^{\mathrm{op2}}\right\|^2$ minimization problem, can be written as below using (18):

$$\mathbf{f}_{\mathrm{P}}^{\mathrm{pr2}} \triangleq \exp\left\{j\,\angle\boldsymbol{\mathcal{G}}^{\mathrm{H}}\,\mathrm{vec}\left\{\mathbf{H}_{\mathcal{SU}}\right\}\right\}. \tag{19}$$

Remark 1 *The proposed EB design for multiuser PET for practical scenarios is obtained by substituting the estimates for $\boldsymbol{\mathcal{G}}$ and $\mathbf{H}_{\mathcal{SU}}$ as respectively defined in* (8) *and* (11)*, in the expression for PIS designs as given by* (15) *or* (19)*, and then finally substituting the resultant in $\mathbf{G}$ to obtain the active EB design $\mathbf{f}_{\mathrm{A}}^{\mathrm{op}}$ as defined in Section 4.1.*

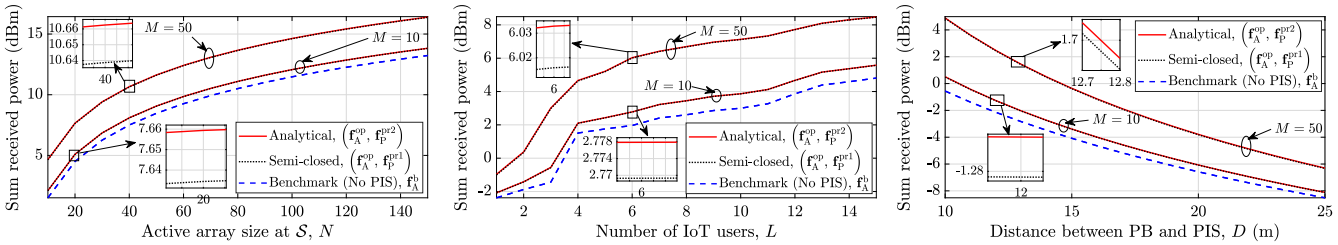

Fig. 2. Comparison of the achievable sum received power performance of the proposed EB designs against the benchmark.

5. NUMERICAL RESULTS AND CONCLUSION

We conduct a numerical investigation to compare the performance of the proposed EB designs for different system parameters and quantify the achievable gains due to PET under CE errors. The default simulation parameters are $N = 10, M = 20, L = 4, \tau = 10$ms and $\tau_c = \frac{0.01\tau}{M+1}$, $\epsilon_1 = 0$, $\epsilon_0 = 10^{-3}$, $p_e = 30$dBm, $p_c = -10$dBm, $\sigma^2_{\mathrm{w}_\mathcal{S}} = \sigma^2_{\mathrm{w}_\mathcal{U}} = \sigma^2 \triangleq 10^{-20}$ Joule (J) [21], $K_{ik} = 10$, and $\beta_{ik} = \frac{G_i G_k \varpi}{d_{ik}^{\varrho}}, \forall i, k \in \{\mathcal{S}, \mathcal{U}, \mathcal{I}\}$, where $\varpi = \left(\frac{\delta}{2\pi}\right)^2$ being average channel attenuation at unit reference distance with $\delta = 0.5\lambda$ being the inter-element separation at PIS and PB [21], $\lambda = 0.328$m [26] being transmit wavelength, d_{ik} is i to k distance, $G_\mathcal{S} = G_\mathcal{U} = 0$dBi, $G_\mathcal{I} = 5$dBi [27], and $\varrho = 2$ is the path loss exponent [28]. Adopting square-field topology [27] for positioning L users with $\mathcal{S}$ and $\mathcal{I}$ being symmetrically placed on the two opposite sides (cf. Fig. 1). Specifically, users are uniformly deployed within a square of length $D = 10$m. Lastly, all results here are generated after taking average over 10^4 independent channel realizations and underlying specular components of Rician channels are modeled using [20, eq. (2)].

5.1. Performance Comparison and Impact of Key Parameters

We start with comparing the performance of the two proposed passive EB designs, namely, (a) semi-closed-form PIS design $\mathbf{f}_{\mathrm{P}}^{\mathrm{pr1}}$, and (b) analytical PIS design $\mathbf{f}_{\mathrm{P}}^{\mathrm{pr2}}$, with active EB being $\mathbf{f}_{\mathrm{A}}^{\mathrm{op}}$, for different values of key system parameters like active array size N at PB, PIS size M, number L of IoT users, and the distance D between PB and PIS. Specifically, Fig. 2 plots the relative sum received power performance for different values of N, L, and D with $M = 10$ and $M = 50$, while assuming perfect CSI availability at $\mathcal{S}$ for designing EB. The benchmark scheme considered here sets its active EB design as $\mathbf{f}_{\mathrm{A}}^{\mathrm{b}} \triangleq \mathrm{v}_{\max}\left\{\mathbf{H}_{\mathcal{SU}}^{*}\,\mathbf{H}_{\mathcal{SU}}^{\mathrm{T}}\right\}$, while assuming no PIS availability.

From Fig. 2(a), we observe that throughout the variation of N from 10 to 150, the average gain as achieved by using $M = 50$ over $M = 10$ remains almost constant around 2.6dB. Also, 11.7 dB gain is achieved by both schemes when N is increased from 10 to 150.

In contrast, as the number L of IoT users increases from 1 to 15 in Fig. 2(b), the sum received power performance improves by 7.65dB and 9.43dB, respectively, for $M = 10$ and $M = 50$, due to larger contributing terms in the sum. Also, the gain achieved by $M = 50$ over $M = 10$ improves with L from 1dB for $L = 1$ to 3dB to $L = 15$. Lastly, with the field size D increased from 10m to 25m, the performance in Fig. 2(c) degrades by 4.5dB and 1.9dB, respectively, for $M = 10$ and $M = 50$, due to larger wireless propagation losses. This performance degrades by -8.6dB and -11.2dB respectively for $M = 10$ and $M = 50$ for two extreme values of D.

5.2. Impact of CE Errors and Concluding Remarks

Now we shift focus from EB design to quantifying the goodness of the proposed LS estimators in Section 3.2 for different values of M and signal-to-noise-ratio (SNR) $\overline{\gamma}_c \triangleq \frac{\beta_{\mathcal{SI}} p_c \tau_c}{\sigma^2}$. Here, since the analytical $\mathbf{f}_{\mathrm{P}}^{\mathrm{pr2}}$ performs better than $\mathbf{f}_{\mathrm{P}}^{\mathrm{pr1}}$, we have used the former one for verifying the CE quality. As observed from Fig. 3, the quality of the proposed estimators improves with increasing $\overline{\gamma}_c$ for both with and without PIS settings because the underlying CE error reduces. In fact for higher SNR value of $\overline{\gamma}_c > 5$dB and $\overline{\gamma}_c > 10$dB, approaches the ideal perfect CSI case respectively for $M = 0$ and $M = 100$.

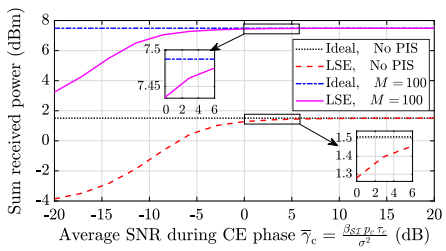

Fig. 3. Validating the quality of proposed LS estimators.

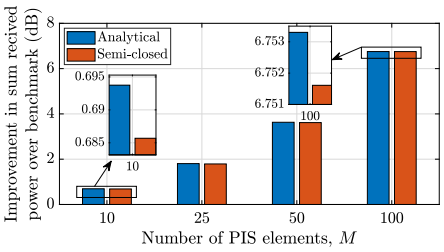

Fig. 4. Gains as achieved by proposed design over benchmark.

Finally, we plot the performance gains as achieved by the two proposed designs over the benchmark one having no PIS in Fig. 4. We notice that although the analytical PIS design is better than the semi-closed-form one, the gap between performance of $\mathbf{f}_{\mathrm{P}}^{\mathrm{pr2}}$ and $\mathbf{f}_{\mathrm{P}}^{\mathrm{pr1}}$ design is in general less than 0.01dB. Furthermore, as compared to the results plotted in Fig. 2, the performance gains are better for practical settings as plotted in Fig. 4 involving usage of LS estimators instead of perfect CSI. In particular, the practical scenario using LS estimators provides an additional improvement of 0.01dB, 0.03dB, 0.06dB, and 0.13dB, for M as 10, 25, 50, and 100, respectively, which signifies the utility of our proposed CE protocol. In general, an improvement of 0.7dB to 6.8dB is achieved by the proposed CE with optimal EB for $M = 10$ and $M = 100$, respectively.

Now we conclude with highlighting the key take-away messages. This paper introduced an *on-off based CE protocol* and derived the *closed-form expressions for the underlying LS estimators* for all the desired channel links. *Novel analytical expressions for the jointly-optimal active and passive EB designs* are proposed that demonstrate *significant performance enhancement over the benchmark design*. The developments of this paper for sustainable IoT settings can be extended for exploring the efficacy of PET in improving information rates and spectral efficiencies in multiuser systems.

6. REFERENCES

[1] F. Liu, O. Tsilipakos, A. Pitilakis, A. C. Tasolamprou, M. S. Mirmoosa, N. V. Kantartzis, D.-H. Kwon, J. Georgiou, K. Kossifos, M. A. Antoniades, M. Kafesaki, C. M. Soukoulis, and S. A. Tretyakov, "Intelligent metasurfaces with continuously tunable local surface impedance for multiple reconfigurable functions," *Phys. Rev. Applied*, vol. 11, no. 4, p. 044024, Apr. 2019.

[2] E. Basar, M. Di Renzo, J. De Rosny, M. Debbah, M. Alouini, and R. Zhang, "Wireless communications through reconfigurable intelligent surfaces," *IEEE Access*, vol. 7, pp. 116 753–116 773, Aug. 2019.

[3] C. Liaskos, S. Nie, A. Tsioliaridou, A. Pitsillides, S. Ioannidis, and I. Akyildiz, "A new wireless communication paradigm through software-controlled metasurfaces," *IEEE Commun. Mag.*, vol. 56, no. 9, pp. 162–169, Sept. 2018.

[4] X. Tan, Z. Sun, J. M. Jornet, and D. Pados, "Increasing indoor spectrum sharing capacity using smart reflect-array," in *Proc. IEEE ICC*, Kuala Lumpur, Malaysia, May 2016, pp. 1–6.

[5] X. Tan, Z. Sun, D. Koutsonikolas, and J. M. Jornet, "Enabling indoor mobile millimeter-wave networks based on smart reflect-arrays," in *Proc. IEEE INFOCOM*, Honolulu, USA, Apr. 2018, pp. 270–278.

[6] S. Hu, F. Rusek, and O. Edfors, "Beyond massive MIMO: The potential of data transmission with large intelligent surfaces," *IEEE Trans. Signal Process.*, vol. 66, no. 10, pp. 2746–2758, May 2018.

[7] S. Nie, J. M. Jornet, and I. F. Akyildiz, "Intelligent environments based on ultra-massive MIMO platforms for wireless communication in millimeter wave and terahertz bands," in *Proc. IEEE ICASSP*, Brighton, UK, May 2019, pp. 7849–7853.

[8] Q. Wu and R. Zhang, "Intelligent reflecting surface enhanced wireless network via joint active and passive beamforming," *IEEE Trans. Wireless Commun.*, pp. 1–16, Aug. 2019, early access.

[9] C. Huang, A. Zappone, M. Debbah, and C. Yuen, "Achievable rate maximization by passive intelligent mirrors," in *Proc. IEEE ICASSP*, Calgary, Canada, Apr. 2018, pp. 3714–3718.

[10] L. Subrt and P. Pechac, "Intelligent walls as autonomous parts of smart indoor environments," *IET Commun.*, vol. 6, no. 8, pp. 1004–1010, May 2012.

[11] S. V. Hum and J. Perruisseau-Carrier, "Reconfigurable reflectarrays and array lenses for dynamic antenna beam control: A review," *IEEE Trans. Ant. Prop.*, vol. 62, no. 1, pp. 183–198, Jan. 2014.

[12] S. Foo, "Liquid-crystal reconfigurable metasurface reflectors," in *Proc. IEEE Int. Symp. on Ant. Prop. (ISAP)*, San Diego, USA, July 2017, pp. 2069–2070.

[13] Y. Han, W. Tang, S. Jin, C. Wen, and X. Ma, "Large intelligent surface-assisted wireless communication exploiting statistical csi," *IEEE Trans. Veh. Tech.*, vol. 68, no. 8, pp. 8238–8242, Aug. 2019.

[14] C. Huang, A. Zappone, G. C. Alexandropoulos, M. Debbah, and C. Yuen, "Reconfigurable intelligent surfaces for energy efficiency in wireless communication," *IEEE Tran. Wireless Commun.*, vol. 18, no. 8, pp. 4157–4170, Aug. 2019.

[15] Q.-U.-A. Nadeem, A. Kammoun, A. Chaaban, M. Debbah, and M.-S. Alouin, "Asymptotic analysis of large intelligent surface assisted MIMO communication," *arXiv:1903.0812*, Apr. 2019.

[16] C. Liaskos, A. Tsioliaridou, A. Pitilakis, G. Pirialakos, O. Tsilipakos, A. Tasolamprou, N. Kantartzis, S. Ioannidis, M. Kafesaki, A. Pitsillides, and I. Akyildiz, "Joint compressed sensing and manipulation of wireless emissions with intelligent surfaces," in *Proc. IEEE DCOSS*, Santorini Island, Greece, May 2019, pp. 318–325.

[17] D. Mishra and H. Johansson, "Channel estimation and low-complexity beamforming design for passive intelligent surface assisted MISO wireless energy transfer," in *Proc. IEEE ICASSP*, Brighton, UK, May 2019, pp. 4659–4663.

[18] ——, "Low-complexity beamforming designs and channel estimation for passive intelligent surface assisted MISO energy transfer," *submitted to IEEE Trans. Commun.*, Feb. 2020.

[19] K. Huang and V. K. N. Lau, "Enabling wireless power transfer in cellular networks: Architecture, modeling and deployment," *IEEE Trans. Wireless Commun.*, vol. 13, no. 2, pp. 902–912, Feb. 2014.

[20] Y. Zeng and R. Zhang, "Optimized training design for wireless energy transfer," *IEEE Trans. Commun.*, vol. 63, no. 2, pp. 536–550, Feb. 2015.

[21] S. Kashyap, E. Björnson, and E. G. Larsson, "On the feasibility of wireless energy transfer using massive antenna arrays," *IEEE Trans. Wireless Commun.*, vol. 15, no. 5, pp. 3466–3480, May 2016.

[22] S. M. Kay, *Fundamentals of Statistical Signal processing: Estimation Theory*. Upper Saddle River, NJ: Prentice Hall, 1993, vol. 1.

[23] M. S. Bazaraa, H. D. Sherali, and C. M. Shetty, *Nonlinear Programming: Theory and Applications*. New York: John Wiley and Sons, 2006.

[24] J. Liang, P. Stoica, Y. Jing, and J. Li, "Phase retrieval via the alternating direction method of multipliers," *IEEE Signal Process. Lett.*, vol. 25, no. 1, pp. 5–9, Jan. 2018.

[25] L. Yang, Y. Zeng, and R. Zhang, "Wireless power transfer with hybrid beamforming: How many RF chains do we need?" *IEEE Trans. Wireless Commun.*, vol. 17, no. 10, pp. 6972–6984, Oct. 2018.

[26] "Powercast datasheet – P1110B Powerharvester receiver," http://www.powercastco.com./documentation/, accessed Oct. 23, 2017.

[27] Q. Wu and R. Zhang, "Intelligent reflecting surface enhanced wireless network: Joint active and passive beamforming design," in *Proc. IEEE GLOBECOM*, Abu Dhabi, UAE, Dec. 2018, pp. 1–6.

[28] D. Mishra and S. De, "Utility maximization models for two-hop energy relaying in practical RF harvesting networks," in *Proc. IEEE ICC*, Paris, France, May 2017, pp. 41–46.